

https://doi.org/10.1070/QEL16386

Formation of high quality interference fringes from both sides of a suitably designed hololens in the laser Doppler anemometer measurement volume

Abhijit Ghosh, A.K. Nirala

Abstract. **We report, for the first time to the best of our knowledge, the formation of high quality, evenly spaced, undistorted fringes in the measurement volume of a laser Doppler anemometer from both sides of a suitably designed hololens. Experiments are performed for the analysis of fringes formed at the measurement volume by real time monitoring and actual fringe field analysis techniques. The results indicate the qualitative as well as quantitative improvement of 66.58% in overall average normalised standard deviations of the width of the fringes formed by the proposed imaging configuration than that of the conventional imaging configuration.**

Keywords: *holographic optical element, laser Doppler anemometry, measurement volume, fringe analysis.*

1. Introduction

The invention of the laser has revitalised the ancient science of optics, injected practical significance into the study of coherent light and aroused new hopes to old ideas. With the developments of lasers, non-intrusive flow measurements became practical. Non-intrusive optically based measurements have given researchers insight into the details of fluid dynamics that could not be obtained with any other technique. The laser anemometer is based on the principle of the Doppler shift; the frequency of the radiation scattered by a seeded particle suspended in the flow moving relative to a radiating source is changed by an amount which depends on the velocity and the scattering geometry. However, the Doppler shift is a very small fraction of the incident frequency, so it causes a high degree of uncertainty in measurements. To improve the estimate of the Doppler shift, a dual beam interference fringe model has been developed. In this model two beams are generated from a single laser source and are then allowed to cross at a point using a converging lens to provide an interference fringe pattern in a region where the measurement of the flow velocity of a fluid is performed. This region is called the measurement volume. When waves of equal amplitude and nearly equal frequency are superimposed, the amplitude of the resulting signal periodically rises and falls. This modulation is called a beat. The beat frequency is twice the modulation frequency or one half the differences between the two original frequencies. The beat frequency is the absolute value of the Doppler shift. In the terminology of laser Doppler anemometry (LDA) measurement techniques, the beat frequency is called the Doppler frequency [1]. The Doppler frequency in the light scattered by the particle passing through the measurement volume can also be calculated by accounting for the interference of laser lights in the measurement volume. The interference of the light beams in the measurement volume creates a set of equally spaced fringes that are parallel to the bisector of the beams. The distance Λ between alternate dark and bright fringes depends on the wavelength λ and angle between the incident beams θ: $\Lambda = \lambda/[2\sin(\theta/2)]$ [2]. A particle suspended in the flow is assumed to pass through the measurement volume and so flickers light when it passes through the bright fringe and no flickering occurs when it comes in contact with the dark fringe. The frequency f of the scattered light when the particle crosses through the fringes can be measured with a photodetector and a signal processing unit. The flow velocity component V perpendicular to the fringe pattern can be calculated from the relation $V = \Lambda f$ [3].

The technological progress has greatly contributed to the advancement of LDA systems and recent new developments in optoelectronic devices provide more accurate measurements, error-free outputs, automation capabilities and other benefits to the LDA users [4–8]. For many of these reasons, the use of LDA methods has become a standard tool for measuring the fluid velocity, on a worldwide basis [9–13]. The complete LDA system can be divided into three sections: optical systems, signal processing systems and data processing systems. In this work, our main interest is focused on the optical system only. The necessary condition for accurate LDA measurements is the evenly spaced, undistorted interference fringe pattern at the measurement volume [14]. Several factors are responsible for fringe distortion and nonuniformity in fringes at the measurement volume: (i) improper optical layout [15]; (ii) astigmatism due to the laser beam refractions [16, 17]; (iii) local fringe distortion caused by laser light diffraction through particles in the transmission path of the laser beams [18]; (iv) curvature effect [19]; (v) optical aberrations caused by the transmitting optics [1]; and (vi) other factors [20]. If two beams intersect at their respective beam waists, wavefronts are approximately planar and consequently the interference will produce parallel planes of bright and dark fringes. If two laser beams do not intersect at the beam waists but elsewhere in the beams, the wave fronts will be curved rather than plane, and as a result the fringe spacing will not be constant but depend on the position within the intersection volume. As a consequence, the measured Doppler frequency will also depend on the particle position, and as

Abhijit Ghosh, A.K. Nirala Biomedical Optics Lab, Department of Applied Physics, Indian Institute of Technology (Indian School of Mines), Dhanbad 826004, Jharkhand, India;
e-mail: abhi.photonics@gmail.com, aknirala@gmail.com

Received 24 March 2017; revision received 6 June 2017
Kvantovaya Elektronika **47** (10) 960–966 (2017)
Submitted in English

such it will no longer be directly proportional to the particle velocity, hence resulting in inaccuracy in measurements [21]. In order to have an undistorted interference fringe pattern at the measurement volume, the imaging lens should ensure diffraction limited performance almost free from all monochromatic aberrations over two small areas encompassed by two apertures on the lens through which two light beams pass. Fringes formed at the measurement volume by a conventional (lens) imaging system become distorted due to the aberration introduced by two small areas encompassed by two apertures [22].

Several authors [23–28] have used a holographic optical system in the LDA optical system to replace the costly and bulky conventional optical system by a light-weight, low cost and aberration free (monochromatic) [29–31] holographic optical system. In previous communications we have reported LDA optical setups consisting of compact two hololenses [31] and a single hololens [28] for improving the fringe quality at the measurement volume.

In present work, we have proposed and applied a suitably designed hololens which can be used from both sides (emulsion as well as opposite side) in the LDA optical setup, which makes the imaging system more versatile. In previously reported hololens imaging system, there is a limitation in utilisation: the hololens can be used from one side only to satisfy the wavefront matching condition. In addition, the proposed hololens imaging system has a higher diffraction efficiency than that of already reported double and single hololens imaging systems because its first order focal point is being utilised for the formation of the LDA measurement volume. Note, however, that the efficiency of the double hololens imaging system will fall down due to utilisation of two hololenses whereas in case of the already reported single hololens, its efficiency is reduced due to utilidation of its second order focal point for generation of the measurement volume. For complete characterisation of the fringes formed at the measurement volume, real time monitoring and another actual fringe field measuring techniques have been applied.

2. Experimental

2.1. Hololens designing

An interferogram of a diverging spherical wavefront with a mutually coherent planar wavefront is a well-known hololens recording geometry reported by many authors [32, 33]. Computer based hologram imagery and other focusing properties of holograms are also found in several papers [34, 35]. In this work we have experimentally investigated and realised a hololens recording geometry which is an interferogram of two spherical wavefronts of different nature: one diverging and the other converging.

The hololens have been recorded using two coherent waves derived from the same laser source. Out of two coherent waves, one is a diverging spherical wavefront generated from a pinhole (at a distance of 20 cm from the plate) and the other is a converging spherical wavefront generated from a converging lens (the distance of the converging point source from the plate was 19.5 cm), as shown in figure 1. The interferogram of diverging and converging spherical wavefronts was recorded on a photosensitive plate. The angle θ between two interfering wavefronts, i.e., diverging and converging spherical wavefronts, was 17° at the time of recording and therefore the corresponding central fringe spacing formed on

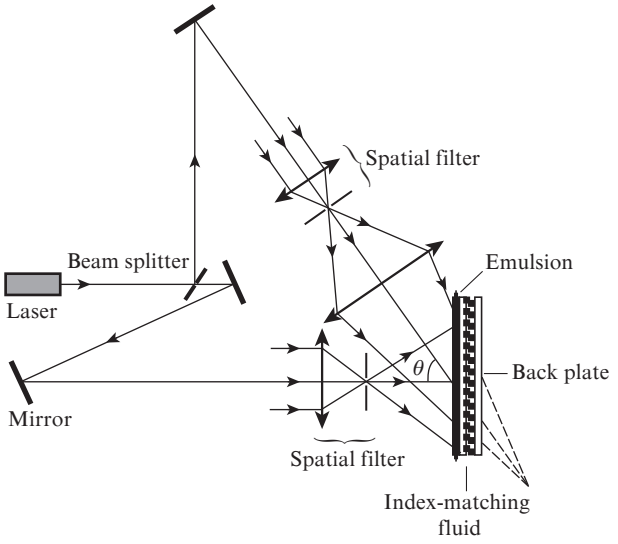

Figure 1. Schematic of the recording geometry for proposed hololens.

the hololens was $\Lambda = 2.14$ μm. The diameter of the recorded hololens was 1.5 cm.

Dichromated gelatin has a high diffraction efficiency, low noise, high resolution, long life and high refractive index modulation capacity [36, 37]; however, due to ease of availability and cost effectiveness of source and recording materials, we have recorded hololens on a commercially available high-resolution silver halide plate PFG-01 [38] (the film thickness is $d = 7$ μm and the average refractive index is $n = 1.61$) using a 17 mW He–Ne laser source ($\lambda = 632.8$ nm). To prevent the formation of a spurious grating, the resulting interference of the two waves should be recorded under the index matched condition [39, 40]. The exposed film was processed using a standard procedure [41, 42].

2.2. LDA optical setup consisting of the proposed hololens imaging configuration

2.2.1. Arrangement for real time monitoring of the fringe field formed inside the LDA measurement volume. In this setup, an expanded laser beam is produced using a spatial filtering arrangement shown in Fig 2. A mask (containing two circular apertures of diameter 1.2 mm, separated by a distance 6.7 mm) is placed for producing two identical pencil light beams in front of an optically recorded hololens which is used for proper intersection of two light beam at its focal point for the formation of an interference fringe pattern at the measurement volume. For characterisation of fringes formed at the measurement volume, a linear CCD camera is placed at 40 cm away from a 20× microscopic objective. The CCD sensor is gradually moved step by step to cover-up the entire profile picture of the measurement volume consists of the interference fringe pattern.

2.2.2. Arrangement for the measurement of the actual fringe field formed inside the LDA measurement volume. For the analysis of the actual fringe field formed inside the measurement volume, an experiment has been carried out (depicted in Fig. 3), in which a photosensitive plate (silver halide plate) has been used at the intersection region of the two beams for recording the fringe pattern of the measurement volume. After suitably exposing the plate, it was processed and

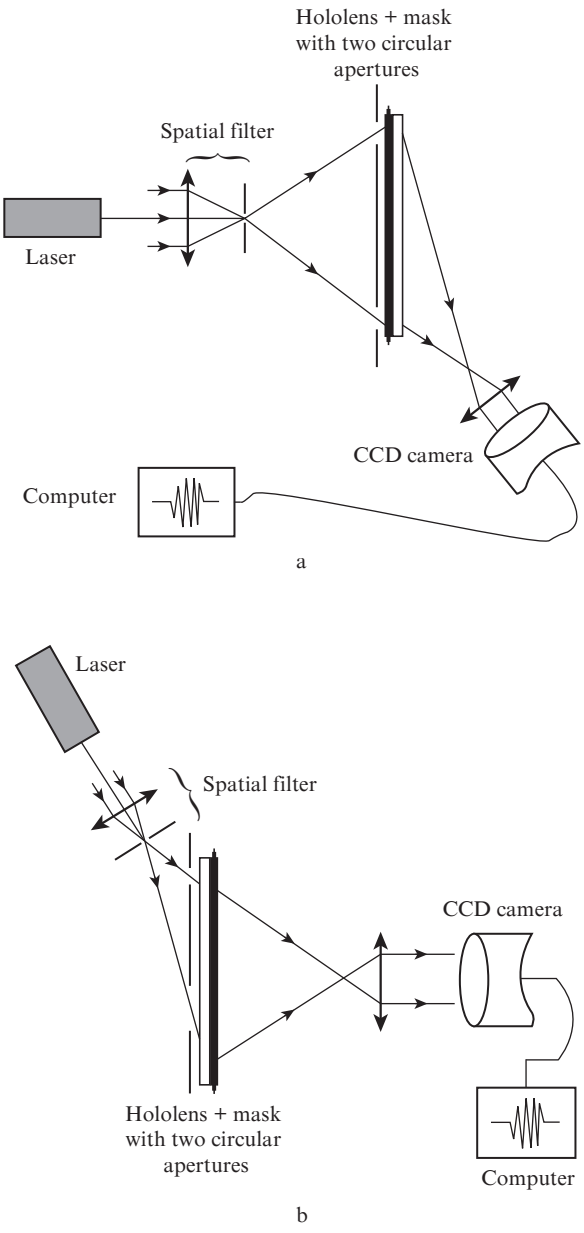

Figure 2. Schematic of the LDA optical setup for real time monitoring of the fringe field formed inside the measurement volume using the proposed hololens illuminated from (a) emulsion side and (b) its opposite side.

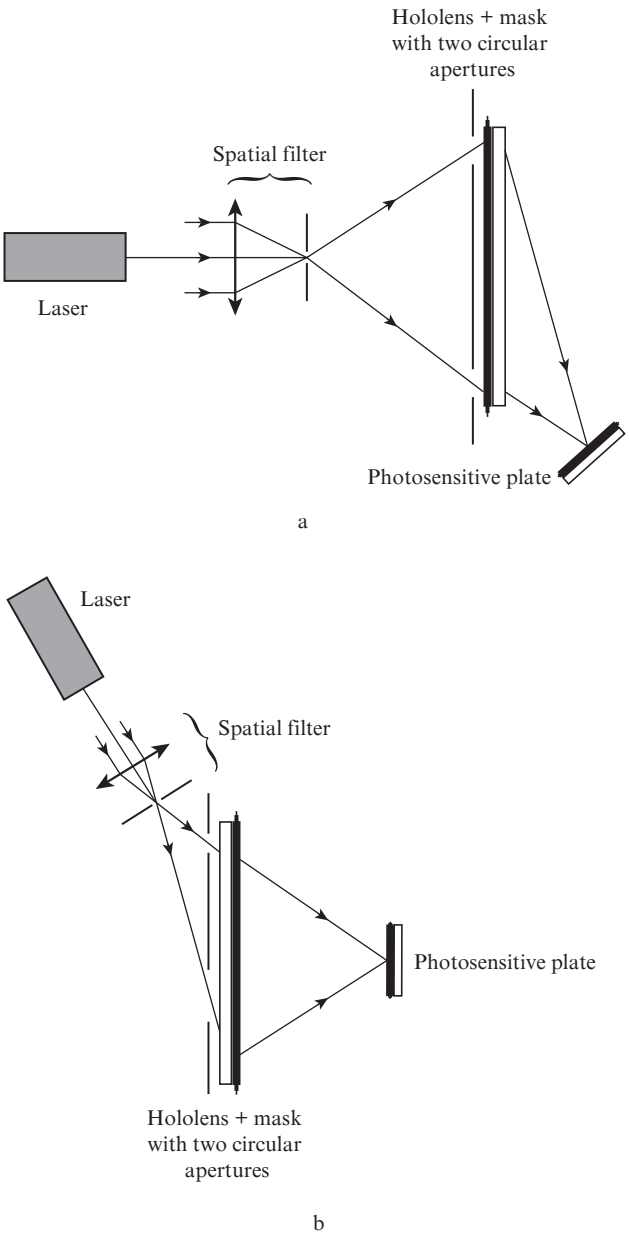

Figure 3. Schematic of the LDA optical setup for analysis of the actual fringe field formed inside the measurement volume using the proposed hololens illuminated from (a) emulsion side and (b) its opposite side.

analysed using a Bruker atomic force microscope (AFM) (Dimension Icon).

3. Results

3.1. Real time monitoring of the fringe field formed inside the LDA measurement volume

Photographs of an optically magnified fringe field of the LDA measurement volume consisting of higher order fringes is shown in Fig. 4. The intensity profile obtained perpendicular to the fringe patterns at various positions of zero order fringe system are shown in Fig. 5 for minute observation and the results of the quantitative analysis presented in Tables 1 and 2.

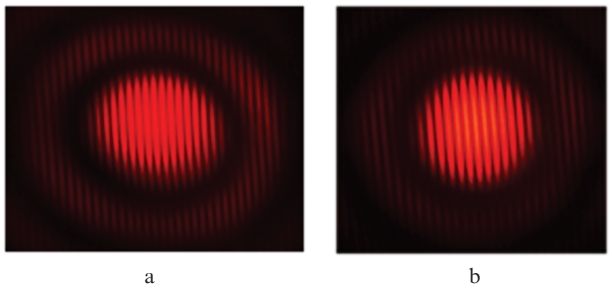

Figure 4. Photographs of the optically magnified fringe field of the LDA measurement volume using the proposed hololens illuminated from (a) emulsion side and (b) its opposite side.

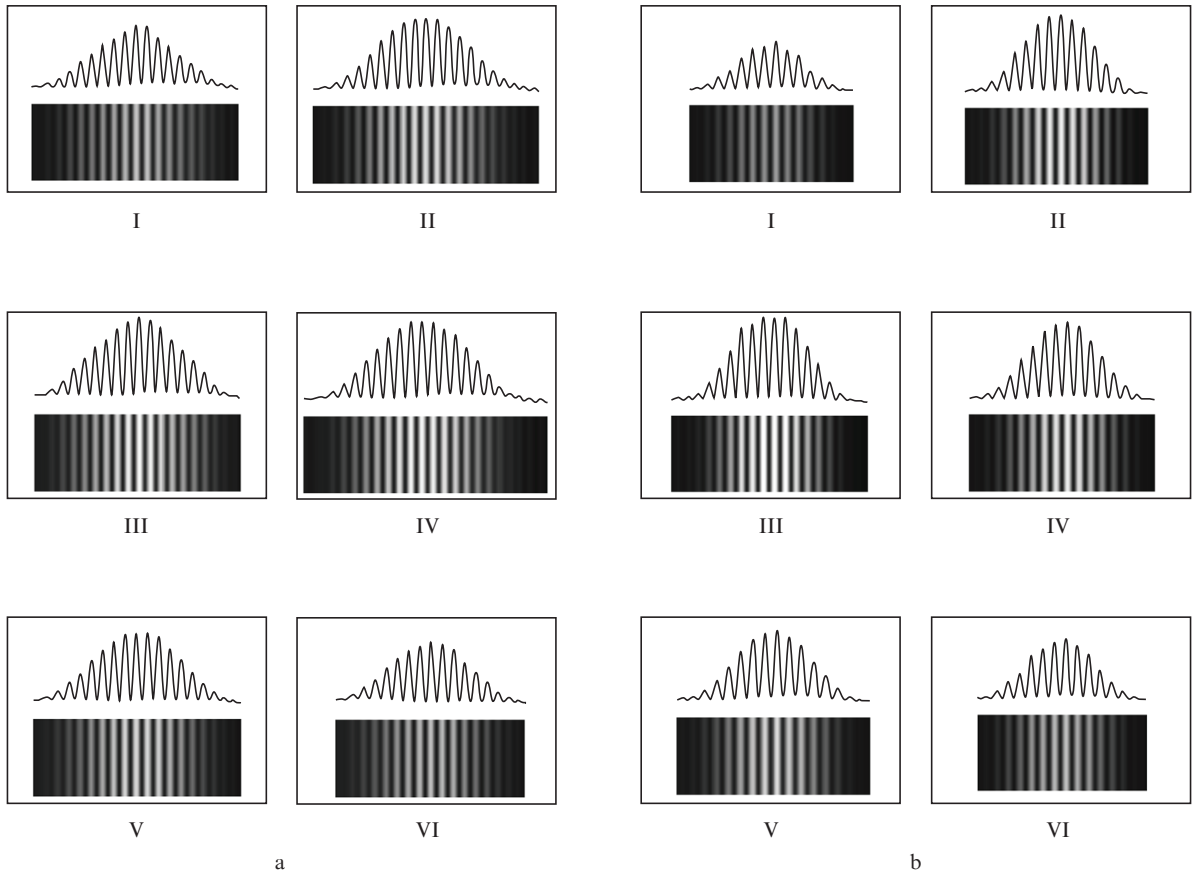

Figure 5. Intensity profile perpendicular to the fringe patterns at various positions of the zero order fringe system shown in (a) Fig. 4a and (b) Fig. 4b, obtained using a linear CCD camera.

It is evident that the quality of the interference fringes obtained using the proposed hololens imaging configuration (shown in Fig. 5) is better compared to that obtained using the conventional imaging configuration [28, 31]. In addition, quantitative analysis presented in Tables 1 and 2 ensures the formation of an evenly spaced undistorted interference fringe pattern at the measurement volume using the proposed hololens imaging configuration.

Table 1. Full width at half maximum (FWHM) of fringes at various positions perpendicular to the interference fringe patterns formed at the LDA measurement volume shown in Fig. 5a. The normalised standard deviation is 0.0090 μm.

Fringe number	Fringe width/μm					
	I	II	III	IV	V	VI
1	462	462	462	462	462	462
2	462	462	462	462	462	462
3	462	462	462	462	462	462
4	462	462	462	462	462	462
5	462	462	462	462	462	462
6	462	462	462	462	462	462
7	462	462	462	476	462	462
8	462	462	462	462	462	462
9	462	462	462	462	462	462
10	462	462	462	462	462	462
11	462	462	462	448	448	448
12	462	462	462	448	448	448

Table 2. Full width at half maximum (FWHM) of fringes at various positions perpendicular to the interference fringe patterns formed at the LDA measurement volume shown in Fig. 5b. The normalised standard deviation is 0.0138 μm.

Fringe number	Fringe width/μm					
	I	II	III	IV	V	VI
1	476	476	476	476	476	476
2	476	448	448	462	476	476
3	476	476	476	476	476	476
4	476	476	490	476	476	476
5	476	476	476	476	476	476
6	476	490	476	476	490	476
7	476	476	476	476	476	476
8	476	476	476	476	476	476
9	476	476	476	476	490	476
10		476	476	476		

3.2. Measurement of the actual fringe field formed inside the LDA measurement volume

The AFM images (through the AFM instrument) of the fringe field formed inside the silver halide plate are shown in Fig. 6. Magnified fragments of AFM images of six different arbitrary positions of the central fringe system are presented in Fig. 7. From the sectional analysis of the fringes shown in Fig. 8, we calculated the fringe widths formed inside the silver halide plate (Tables 3 and 4). From 2D AFM images shown

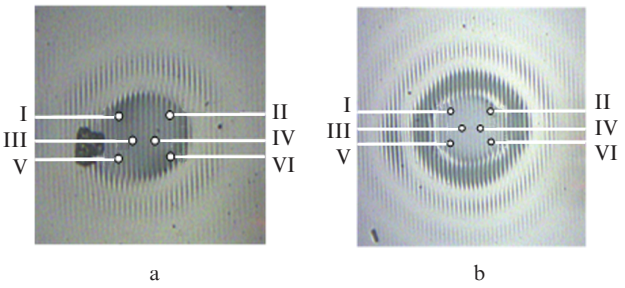

Figure 6. Zero- and higher-order AFM images (through the AFM instrument) of the recorded interference fringe pattern formed at the LDA measurement volume on a silver halide plate using the proposed hololens illuminated from (a) emulsion side and (b) its opposite side.

Table 3. Fringe width at various positions of interference fringe patterns of the LDA measurement volume (measured from sectional analysis of 2D AFM images, shown in Fig. 7a). The normalised standard deviation is 0.0133 μm.

Fringe number	Fringe width/μm					
	I	II	III	IV	V	VI
1	18.431	17.684	18.194	18.421	18.421	18.421
2	18.431	17.693	18.189	18.421	18.421	18.431
3	18.431		18.194	18.421	18.421	18.421

Table 4. Fringe width at various positions of interference fringe patterns of the LDA measurement volume (measured from sectional analysis of 2D AFM images, shown in Fig. 7b). The normalised standard deviation is 0.0161 μm.

Fringe number	Fringe width/μm					
	I	II	III	IV	V	VI
1	19.193	19.195	19.167	18.431	19.195	19.167
2	19.195	19.167	19.167	18.431	19.167	19.168
3	19.168		19.167	18.431		

in Fig. 7 and data presented in Table 3 and 4 it is clear that evenly spaced undistorted interference fringes can easily be formed using the proposed hololens imaging configuration.

Overall average normalised standard deviations of the fringe width formed by the proposed hololens imaging configuration is 0.0130 μm, whereas the corresponding value for the conventional imaging configuration is 0.0389 μm.

4. Discussion and conclusions

The proposed hololens imaging configuration in the LDA optical setup is better in many respect from other reported imaging configurations because of following reasons:

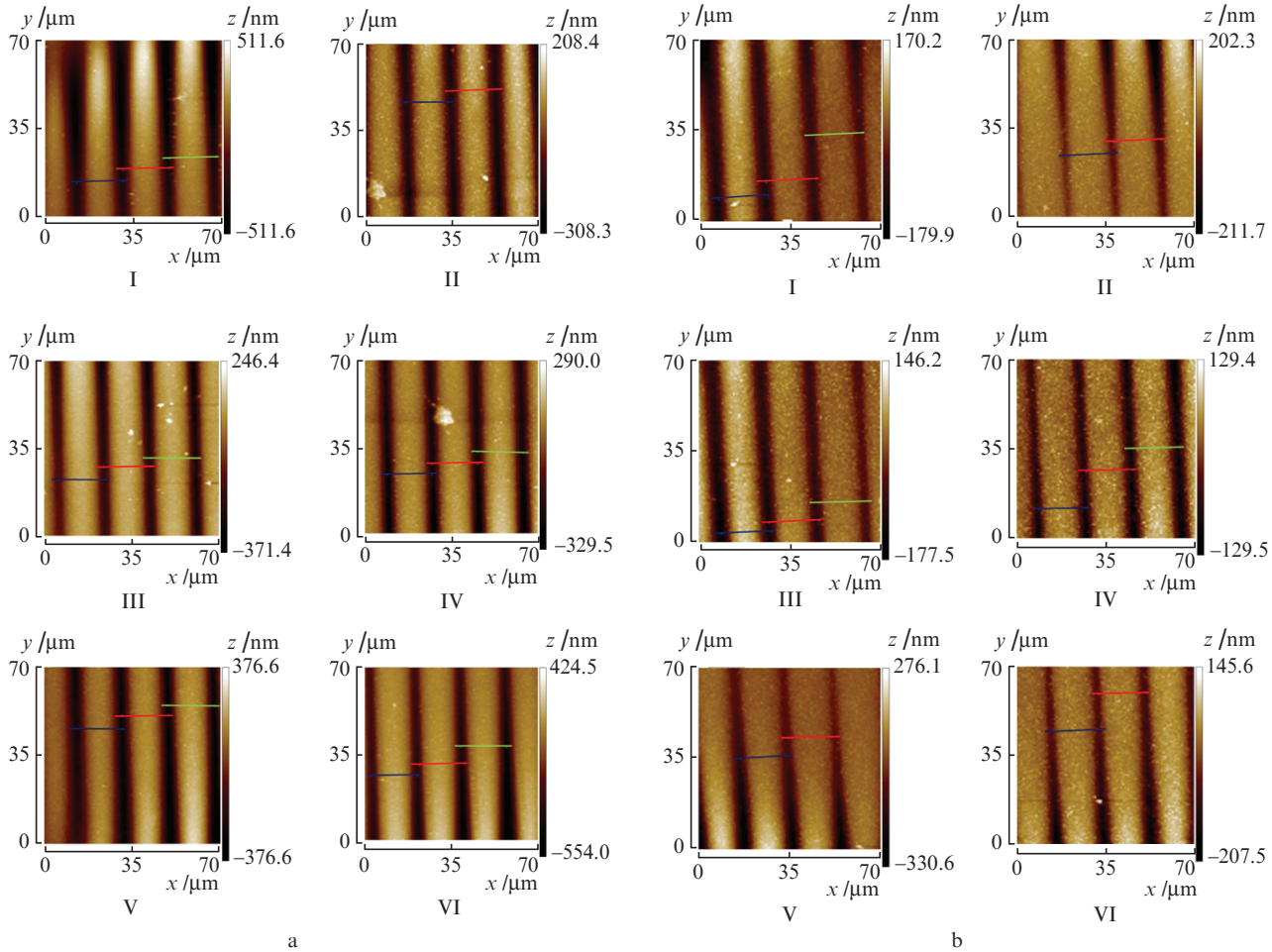

Figure 7. 2D AFM images (size 70 × 70 μm) of zero-order fringes shown in (a) Fig. 6a and (b) Fig. 6b.

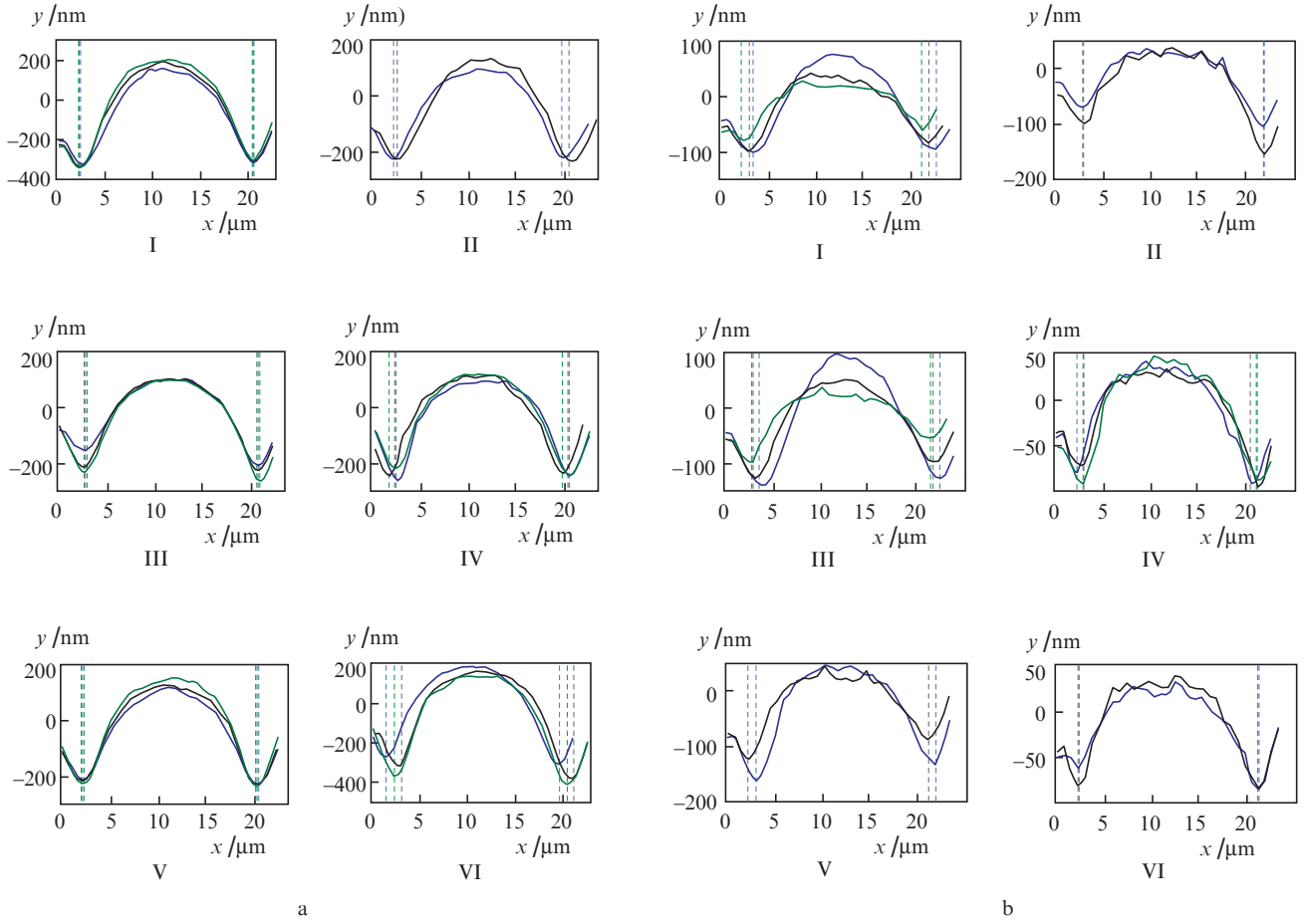

Figure 8. Sectional analysis of fringes across the lines drawn in (a) Fig. 7a and (b) Fig. 7b for fringe width measurement.

(i) There is a significant improvement (66.58%) in overall average normalised standard deviations of the fringe width formed inside the measurement volume over the conventional imaging configuration.

(ii) The number of degrees of freedom is reduced and hence alignment difficulty, bulkiness and cost effectiveness are less as compared to the double hololens imaging configuration.

(iii) The efficiency is higher than that of the existing single hololens imaging configuration because the first-order focal point of the proposed hololens imaging configuration is being utilised.

(iv) The proposed system is easier to fabricate, compact, light weight, cheaper and requires a laser of lesser output wattage than that of the combined hololens in the LDA system.

(v) An additional advantage over all the reported holographic imaging configurations is that it can be utilised from both sides (emulsion as well as opposite side of the plate).

Thus, a properly designed holographic imaging configuration consisting of the proposed hololens has a potential capability to form a high-quality, evenly spaced undistorted interference fringe pattern at the measurement volume and therefore the system may advantageously be implemented in the LDA optical setup to improve the measurement accuracy.

Acknowledgements. The authors would like to thank the Central Research Facility of the Indian Institute of Technology (Indian School of Mines), Dhanbad, for providing an AFM facility for studies.

References

1. Zhang Z. *LDA Application Method Laser Doppler Anemometry for Fluid Dynamics* (Berlin: Springer, 2010).
2. Durst F., Melling A., Whitelaw J.H. *Principles and Practice of Laser Doppler Anemometry* (London: Academic, 1981).
3. Annoni M. *Measurement*, **45**, 1639 (2012).
4. Goldstein R.J. *Fluid Mechanics Measurements* (London: Taylor and Francis, 1996).
5. Albrecht H.-E., Damaschke N., Borys M., Tropea C. *Laser Doppler and Phase Doppler Measurement Techniques* (Berlin: Springer, 2003).
6. Tropea C. *Meas. Sci. Technol.*, **6**, 605 (1995).
7. Czarske J.W. *Meas. Sci. Technol.*, **17**, R71 (2006).
8. Diasinos S., Beves C., Barber T. *Meas. Sci. Technol.*, **24**, 017001 (2013).
9. Butefisch K.-A. *Progr. Aerosp. Sci.*, **26**, 79 (1989).
10. Cagniot A., Cape E.G., Walker P.G., Yoganathan A.P., Levine R.A. *J. Am. Soc. Echocardiogr.*, **5**, 393 (1992).
11. Chandrasekaran M., Marcroft H., Bakalis S., Karwe M.V. *Trends Food Sci. Technol.*, **8**, 369 (1997).
12. Pfeifer C., Bruzzese C., Fast G., Kuhn D., Class A.G. *Flow Meas. Instrum.*, **22**, 456 (2011).
13. Spelter L.E., Schirner J., Nirschl H. *Chem. Eng. Sci.*, **66**, 4020 (2011).
14. Zhang Z., Eisele K. *J. Exp. Fluids*, **25**, 371 (1998).
15. Hanson S. *J. Phys. D: Appl Phys.*, **6**, 164 (1973).
16. Zhang Z., Eisele K. *J. Exp. Fluids*, **20**, 466 (1996).
17. Zhang Z., Eisele K. *J. Exp. Fluids*, **19**, 89 (1995).

18. Ruck B. *J. Exp. Fluids*, **10**, 349 (1991).
19. Huisman S.G., Gils D.P.M.V., Sun C. *Eur. J. Mech. B*, **36**, 115 (2012).
20. Durst F., Stevenson W.H. *Appl. Opt.*, **18**, 516 (1979).
21. Li E., Tieu K., Mackenzie M. *Opt. Las. Eng.*, **27**, 395 (1997).
22. Ghosh A., Nirala A.K. *Meas. Sci. Technol.*, **27**, 055202 (2016).
23. Stojanoff C.G., Tholl H.D., Luebbers H.A., Windeln W. *Proc. SPIE*, **1507**, 426 (1991).
24. Schneider F., Windein W. *Appl. Opt.*, **27**, 4481 (1988).
25. Hansen C.D., Kitchen S.R. *Opt. Las. Eng.*, **44**, 954 (2006).
26. Schock H.J., Case S., Konicek L. *Appl. Opt.*, **23**, 752 (1984).
27. Connelly M.J., Szecowka P.M., Jallapuram R., Martin S., Toal V., Whelan M.P. *Opt. Lett.*, **33**, 330 (2008).
28. Ghosh A., Nirala A.K. *Laser Phys.*, **25**, 116201 (2015).
29. Meier R.W. *J. Opt. Soc. Am.*, **55**, 987 (1965).
30. Champagne E.B. *J. Opt. Soc. Am.*, **57**, 51 (1967).
31. Ghosh A., Nirala A.K. *Opt. Spectrosc.*, **118**, 482 (2015) [*Opt. Spektrosk.*, **118**, 508 (2015)].
32. Schwar M.J.R., Pandya T.P., Weinberg E.J. *Nature*, **215**, 239 (1967).
33. Richter A.K., Carlson F.P. *Appl. Opt.*, **13**, 2924 (1974).
34. Latta J.N. *Appl. Opt.*, **10**, 599 (1971).
35. Vlasov N.G., Mosyakin Yu.S., Skrotskii G.V. *Sov. J. Quantum Electron.*, **2**, 8 (1972) [*Kvantovaya Elektron.*, (**7**), 14 (1972)].
36. Chang B.J., Leonard C.D. *Appl. Opt.*, **18**, 2407 (1979).
37. Guenther B.D., Steel D. (Eds) *Encyclopedia of Modern Optics* (London: Elsevier Acad. Press, 2005).
38. http://www.integraf.com/Downloads/PFG-01.pdf.
39. Syms R.R.A., Solymar L. *Appl. Phys. B*, **32**, 165 (1983).
40. Shakher C., Yadav H.L., Nirala A.K. *J. Opt.*, **20**, 259 (1989).
41. Saxby G. *Practical Holography* (London: Prentice Hall, 1988).
42. Collier R.J., Burckhardt C.B., Lin L.H. *Optical Holography* (New York: Academic, 1971).